Electrostatic, Thermal and Vapor Density Fields Surrounding Stationary Columnar Ice Crystals

P. K. WANG, C. H. CHUANG AND N. L. MILLER

Department of Meteorology, University of Wisconsin, Madison, WI 53706

(Manuscript received 10 October 1984, in final form 21 June 1985)

ABSTRACT

Formulas suitable for calculating the electrostatic, temperature, and vapor density fields surrounding stationary columnar ice crystals are derived. Columnar ice crystals are approximated as circular cylinders of finite lengths. In this way the effects of sharp edges are taken into account. Results of electrostatic fields for some columnar ice crystals are shown. The potential distribution of a prolate spheroid is also determined and compared to that of a circular cylinder. The results show that the approximation of a columnar crystal by a prolate spheroid is inadequate. Formulas are also given to convert the electric fields into temperature and vapor density fields.

1. Introduction

In many calculations of cloud physics it is often necessary to know the fields of temperature, vapor density, and electric charge distributions surrounding ice crystals. The first two fields are important to the calculations of diffusional growth. Although the classical electrostatic analog method can predict the total diffusional growth rates in which a detailed knowledge of field distributions is unnecessary, it cannot predict the growth habit of ice crystals which depends on these detailed distributions (Pruppacher and Klett, 1978). The knowledge of temperature and vapor density fields is also necessary to the calculations of thermo- and diffusiophoretic forces which are important to the capture of submicron aerosol particles by snow crystals (Grover *et al.*, 1977; Wang *et al.*, 1978; Wang and Pruppacher, 1980). The electrostatic fields are important in calculations such as the charging of snow crystals by ions, scavenging of charged aerosol particles by charged snow crystals, and the collisional growth of snow crystals due to charge effects.

Since snow crystals fall relative to the air, they generate hydrodynamic flow fields surrounding themselves. These flow fields have no effect on the electrostatic fields due to the charges on the snow crystals. Therefore, the calculation of the electrostatic fields can be obtained by solving the Poisson equation in which the flow fields play no part. The calculation of the temperature and vapor density fields, however, do involve the flow fields and, therefore, the appropriate equation here is the convective diffusion equation (see Pruppacher and Klett, 1978). Unfortunately, the flow fields passing snow crystals in atmospheric conditions are not available at present. In this paper we, therefore, limit our treatment to the case of stationary ice crystals. For stationary crystals, the convective diffusion equation becomes the same as the Poisson equation in the electrostatic case. Since many laboratory investigations of the physical properties of ice crystals are carried out under nonflow conditions, it is expected that the results obtained here will be useful to these cases.

In this paper we investigate only the columnar crystals. The true shape of these columns are hexagonal, which is very difficult to treat. We shall approximate these columns by circular cylinders of equal diameter and length. This approximation should represent an improvement to the prolate spheroid approximation which lacks sharp edges at both ends. Even with such a simplification the present problem is still not simple. The main difficulty involved here is that such a cylinder consists of two types of boundary surfaces, namely, the cylindrical side surface and planar end surfaces. This poses a mixed boundary problem and the usual orthogonal function techniques become helplessly complicated. In the present study we apply a technique developed by Smythe (1956, 1962) who use the series expansion and integral transformation method to determine the charge density distribution and capacitance of a charged right circular cylinder. Here we extend his method to derive an analytical expression of the potential distribution which can represent either electric potential, temperature, or vapor density fields surrounding such a cylinder. In Section 2 we shall formulate and calculate the electrostatic fields. Conversions of temperature and vapor density fields will be given at the end.

2. Mathematical formulation

Figure 1 shows the configuration of the cylinder and nomenclature of the problem. Our task is to determine

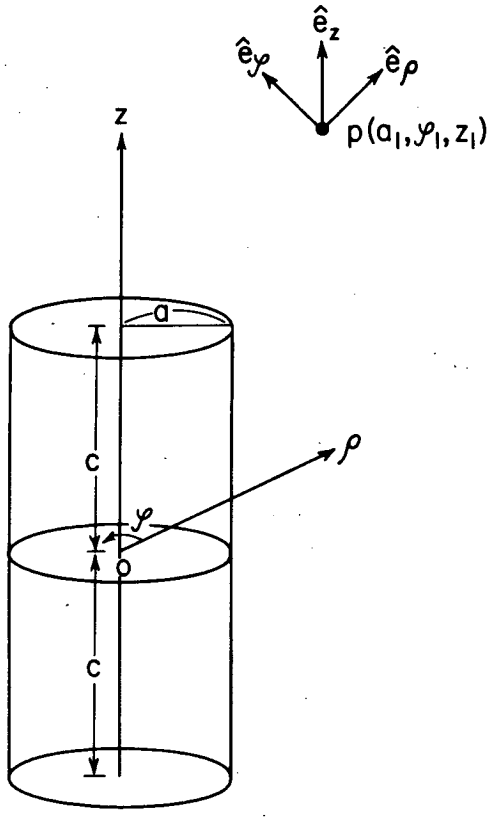

FIG. 1. Nomenclature of the problem. The radius and half-length of the cylinder are a and c, respectively; ρ is the radial coordinate, z the vertical coordinate, $\hat{e}_\rho$, $\hat{e}_\phi$ and $\hat{e}_z$ the unit vectors in radial, azimuthal, and vertical directions, respectively.

the field strength at any outside point $P(a_1, \phi_1, z_1)$. We shall assume that the cylinder is conducting and that it is charged to surface potential V_0. This may be valid for a single crystalline columnar ice. The charge densities on the side and end surfaces can be expressed as (Smythe, 1956; Wang and Chuang, 1982):

$$\sigma_s = \sum_{n=0}^{\infty} A_n(b^2 - z_0^2)^{n-1/3}, \tag{1}$$

and

$$\sigma_e = \sum_{n=0}^{\infty} B_n(1 - \rho_0^2)^{n-1/3}, \tag{2}$$

respectively, where b, z_0, and ρ_0 are dimensionless quantities defined by

$$b = c/a, \quad z_0 = z/c, \quad \text{and} \quad \rho_0 = \rho/a, \tag{3}$$

where a is the radius and c the half-length of the cylinder, ρ and z are the radial and vertical coordinates, respectively, and A_n and B_n are coefficients to be determined. The above charge distributions are such that the following equations are satisfied on a closed surface enclosing the origin:

$$\left(\frac{d^{2p}V(z, 0)}{dz^{2p}}\right)_{z=0} = \begin{cases} V_0 & \text{when} \quad p = 0 \\ 0 & \text{when} \quad p \neq 0, \end{cases} \tag{4}$$

where V is the potential.

As indicated by Smythe (1956), very near the edge the charge distributions (1) and (2) become equal and approach that on the charged rectangular wedge which is proportional to $\delta^{-1/3}$ where δ is the distance from the edge. The property of such a wedge is given in Smythe (1968).

The next step is to determine the coefficients A_n and B_n. This is done first by calculating the potential on the axis of the cylinder due to the charge densities of Eqs. (1) and (2). The expression of the potential is then differentiated with respect to z_0 and finally z_0 is equated to zero (see Smythe (1968) for detail). The result is

$$\frac{d^{2p}V}{dz_0^{2p}} = \sum_{n=0}^{\infty} \left(\frac{MB_n}{n + \frac{2}{3}} F_1 + MNGA_nF_2\right), \tag{5}$$

where

$$M = \frac{\frac{1}{2}a(2p)!}{\epsilon(1 + b^2)^{p+1/2}},$$

$$N = \frac{b^{2n+1/3}\left(n - \frac{1}{3}\right)!\left(p - \frac{1}{2}\right)!}{(-1)^p 2^{2/3}\left(n + \frac{1}{6}\right)!p!},$$

$$G = 0.684463408, \tag{6}$$

and

$$F_1 = F_1\left[p + \frac{1}{2}, n - p + \frac{2}{3}; n + 1 + \frac{2}{3}; (1 + b^2)^{-1}\right],$$

$$F_2 = F_2\left[p + \frac{1}{2}, n - p + \frac{2}{3}; n + 1 + \frac{1}{6}; b^2(1 + b^2)^{-1}\right] \tag{7}$$

are two hypergeometric functions. Equation (5) can be substituted into Eq. (4). This yields a number of simultaneous equations which can be used for solving coefficients A_n and B_n. But we still need an extra condition to relate A_0 and B_0. This additional condition is

$$A_0 = b^{1/3}B_0, \tag{8}$$

so that the charge distributions σ_s and σ_e match at the edge of the cylinder. Thus by solving a number of simultaneous equations of the type of Eq. (5) plus Eq. (8), the coefficients A_n and B_n can be determined. The number of A_n and B_n required to achieve good accuracy (so that the correct surface potential is reproduced) needs not be too large, being 6–8 terms usually.

We now derive an expression for the electric potential outside the cylinder based on the charge density distributions (1) and (2). We first have to determine

the distance r from a point $B(a, \phi, z)$ on the cylinder to the field point $P(a_1, \phi_1, z_1)$. This is (see Fig. 1)

$$r = [(z - z_1)^2 + a^2 + a_1^2 - 2aa_1 \cos(\phi_1 - \phi)]^{1/2}. \quad (9)$$

The contribution of the charges on the cylindrical side surface to the potential at P is therefore

$$V_s(a_1, \phi_1, z_1) = \int_s \frac{\sigma_s}{4\pi\epsilon r}\, ds, \qquad \sum A_n\left(\frac{c^2 - z^2}{a^2}\right)^{n-1/3} ad\phi dz = \int_s \frac{}{4\pi\epsilon[(z_1 - z)^2 + a^2 + a_1^2 - 2aa_1 \cos(\phi_1 - \phi)]^{1/2}}, \quad (10)$$

where $ds = ad\phi dz$ is a surface element on the side surface. The angular part can be readily integrated to give

$$V_s(a_1, \phi_1, z_1) = \frac{1}{4\pi\epsilon}\left[2a \int_{-c}^{c} \sum A_n\left(\frac{c^2 - z^2}{a^2}\right)^{n-1/3} \times \frac{2}{(\alpha_1^2 + \beta_1^2)^{1/2}} K\left(\frac{2\beta_1^2}{\alpha_1^2 + \beta_1^2}\right)^{1/2} dz\right], \quad (11)$$

where the complete elliptic integral K can be expressed as

$$K(k) = \frac{\pi}{2}\left[1 + \left(\frac{1}{2}\right)^2 k^2 + \left(\frac{1 \times 3}{2 \times 4}\right)^2 k^4 + \left(\frac{1 \times 3 \times 5}{2 \times 4 \times 6}\right)^2 k^6 + \cdots\right], \quad k^2 \leq 1, \quad (12)$$

and

$$\left.\begin{aligned} \alpha_1^2 &= (z_1 - z)^2 + a^2 + a_1^2 \\ \beta_1^2 &= 2aa_1 \end{aligned}\right\}. \quad (13)$$

By a similar consideration, the contributions of the charges on upper and lower planar end surfaces to the potential at P are, respectively,

$$V_{e,u}(a_1, \phi_1, z_1) = \int_s \frac{\sigma_e}{4\pi\epsilon r}\, ds = \frac{1}{4\pi\epsilon}\left\{2 \int_0^a \left[\sum B_n\left(\frac{a^2 - \rho^2}{a^2}\right)^{n-1/3}\right] \times \frac{2\rho}{(\alpha_2^2 + \beta_2^2)^{1/2}} K\left(\frac{2\beta_2^2}{\alpha_2^2 + \beta_2^2}\right)^{1/2} d\rho\right\}, \quad (14)$$

and

$$V_{e,l}(a_1, \phi_1, z_1) = \frac{1}{4\pi\epsilon}\left\{2 \int_0^a \left[\sum B_n\left(\frac{a^2 - \rho^2}{a^2}\right)^{n-1/3}\right] \times \frac{2\rho}{(\alpha_3^2 + \beta_2^2)^{1/2}} K\left(\frac{2\beta_2^2}{\alpha_3^2 + \beta_2^2}\right)^{1/2} d\rho\right\} \quad (15)$$

where

$$\left.\begin{aligned} \alpha_2^2 &= (z_1 - c)^2 + a_1^2 + \rho^2, \quad \beta_2^2 = 2a_1\rho \\ \alpha_3^2 &= (z_1 + c)^2 + a_1^2 + \rho^2 \end{aligned}\right\}. \quad (16)$$

The electric potential at an external point $P(a_1, \phi_1, z_1)$ due to the charged circular cylinder is therefore the sum of the above three parts (11), (14), and (15), i.e.,

$$V_P = V_s + V_{e,u} + V_{e,l}. \quad (17)$$

The integrals (11), (14) and (15) are to be calculated by numerical methods.

Once the potential profiles are known, the electric fields can be calculated by taking the gradients of the potentials. In the present paper, these gradients are taken numerically. One can, of course, determine the fields graphically. It is most convenient to use spline interpolation to find the neighboring V values once certain base point potentials are known. It is found that the potentials determined this way are very close to the values calculated using the full expressions. The difference is only on the order of 1%.

3. Results and discussion

Eight cases of cylinders were calculated. These correspond to the eight columnar ice crystals in Schlamp *et al.* (1975) and Wang and Pruppacher (1980). The half-length-to-radius ratios (c/a) used in the calculations are 1.21, 1.43, 1.54, 1.67, 2.22, 3.33, 5.00, and 8.33, with approximate Reynolds numbers 0.2, 0.5, 0.7, 1.0, 2.0, 5.0, 10.0, and 20.0, respectively. Some examples are presented here. All results shown are in SI units. Figures 2 and 3 show the computed charge density distributions (in Coulomb per meter square) on the planar end surfaces and cylindrical side surfaces, respectively. All the cylinders are assumed to be charged to a surface potential of 1 V. To obtain the cases when surface potential is V_0 V, one merely has to multiply the results shown here by the factor V_0. In these and the following figures R represents the radial distance from the z-axis. Obviously the charge densities approach infinity near the edges, as would be expected. This is due to our assumption that edges are infinitely sharp. Also it is clear that over most parts of both end and side surfaces the charge densities are fairly uniform. Only near the edges do the charge densities change rapidly. This behavior allows one to treat most of the surfaces as uniformly charged surfaces. One would therefore expect that the motion of a small particle (small as compared to the dimension of the surface) near the center part of the end surface will be similar to that near a charged infinite plane, while the motion near the equator of the cylindrical surface will be similar to that near a charged infinitely long cylinder.

Figures 4 and 5 show the distribution of potential fields (in volts). Curves 1 to 3 represent the potentials

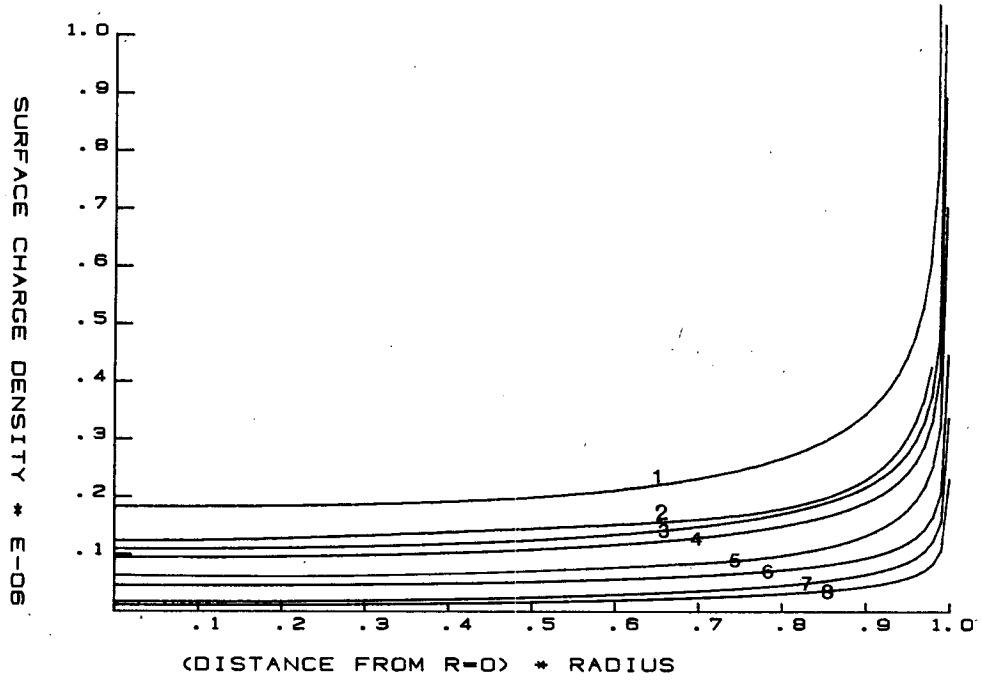

FIG. 2. Distributions of charge density σ_e (in C/m^2) on the end surface. Curve 1, b = 1.21; 2, b = 1.43; 3, b = 1.54; 4, b = 1.67; 5, b = 2.22; 6, b = 3.33; 7, b = 5.00; and 8, b = 8.33.

at z = 0, 0.5c, and 1.0c, respectively. Curve 2 is often very close to curve 1 and therefore is not shown in some cases. As expected, the potentials fall off with increasing distance from the cylinder, the rates of fall (dV/dr, where r is measured in units of a) being larger for shorter cylinders. Also the potentials converge to

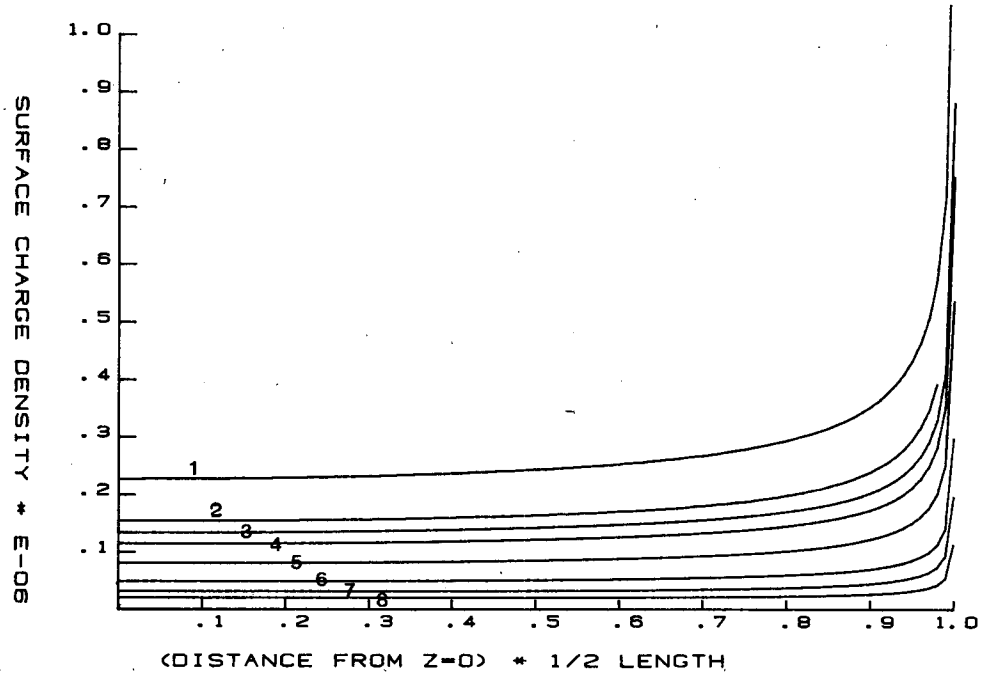

FIG. 3. Distributions of charge densities σ_s (in C/m^2) on the side surface. Labels of curves are the same as Fig. 2.

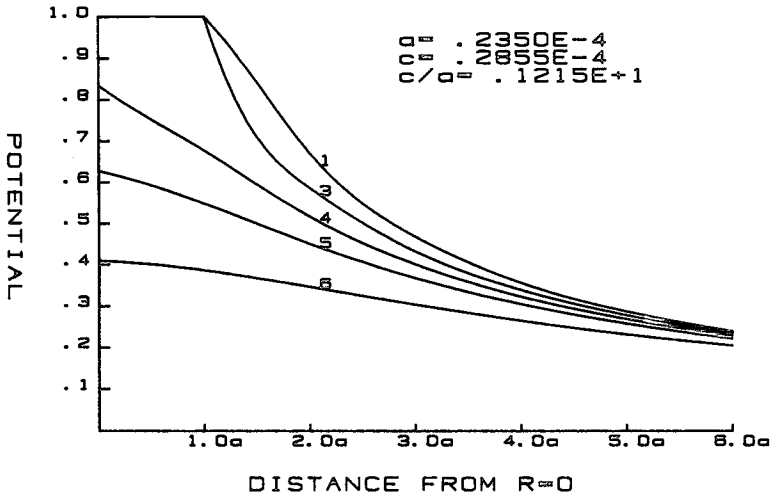

FIG. 4. Profiles of the electric potentials for $b = 1.21$. Curve 1, $z = 0$; 2, $z = 0.5c$; 3, $z = 1.0c$; 4, $z = 1.5c$; 5, $z = 2.0c$; 6, $z = 3.0c$.

one value when far away from the cylinder regardless of the z. This is, of course, due to the fact that when viewed at a distance sufficiently far from the cylinder, any finite cylinder will look like a point charge, and therefore the equipotential surfaces approach concentric spheres. The convergences are faster for the shorter cylinder because one need not go too far to view it as a point charge. One can also think that they are closer to the shape of spheres.

Figures 6 and 7 show the magnitudes of the electric fields (in volts per meter). There is also a convergence feature similar to that of potentials, and can be explained in the same manner. Curve-3 is the field at $z = 1.0c$, its value at $R = 1.0a$ being infinite. This is of course due to the sharp edges in our assumption. Figures 8 and 9 show the zenith angles of the electric fields at different positions. The zenith angle is the angle between the electric field vector and the z-axis. If the field vector is pointing vertically upward (i.e., along the z-axis) then the zenith angle is zero. Since the electric field is azimuthally symmetric, this angle alone is sufficient to determine the direction of the electric field. These angles together with the magnitudes given in Figs. 6 and 7 completely determine the electric field vector. Figure 10 shows an example of the patterns of the field lines. Such configurations make it clear that the very strong fields near the sharp edges shall have important influence on the dynamical behavior of small charged particles getting close to them.

Since prolate spheroids have been considered as good approximations of columnar ice crystals previously, it is instructive to compare their field distributions with

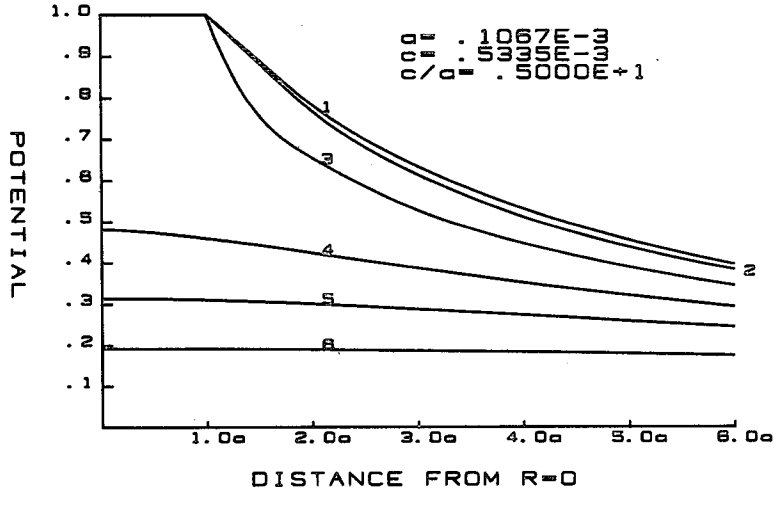

FIG. 5. As in Fig. 4 except for $b = 5.00$.

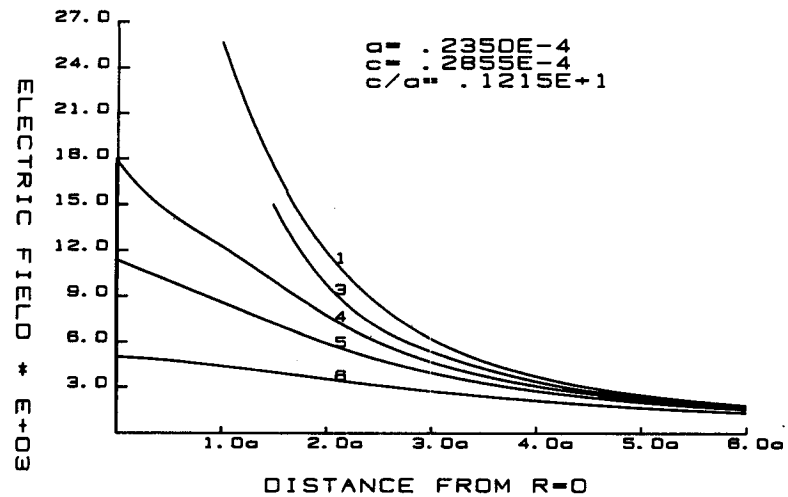

FIG. 6. Profiles of the magnitudes of the electric fields for $b = 1.21$. Labels of curves are as in Fig. 4.

the present cases. Figure 11 provides a comparison between the potential distributions of a circular cylinder and a prolate spheroid. The semimajor and semiminor axes of the prolate spheroid correspond to the half length and the radius of the cylinder, respectively. The potential distribution external to a conducting prolate spheroid charged to a surface potential of 1 V is (Morse and Feshbach, 1953):

$$V = \ln[(\xi + 1)/(\xi - 1)]/\ln[(\xi_0 + 1)/(\xi_0 - 1)], \quad (18)$$

where $\xi = (r_1 + r_2)/f$ is the generalized radial coordinate in a prolate spheroidal coordinate system; ξ = constant being a prolate spheroid with interfocal distance f; r_1 and r_2 are the distances from an external point P to the two foci; ξ_0 is the surface of the prolate spheroid and is equal to $2c/a$ where c and a are the semimajor and semiminor axes of the spheroid. It is seen from Fig. 11 that there are clear discrepancies of the potentials of a prolate spheroid from that of a circular cylinder both in the magnitudes and fall-off rates. For example the potential of the spheroid at $r = 3.0a$ from the equator is ~0.35V while that of a circular cylinder is ~0.47V, a difference of about 34%. This also means that the temperature and vapor density (which are analogous to the electric potential) at this point surrounding a prolate spheroid will also be 34% lower than that of a circular cylinder. In addition, because of the steeper slopes of the potential curves for a prolate spheroid, the electric fields (and hence the heat and vapor fluxes) are overestimated. Since the electric fields and the heat and vapor fluxes represent the strengths of electric, thermophoretic, and diffusiophoretic forces,

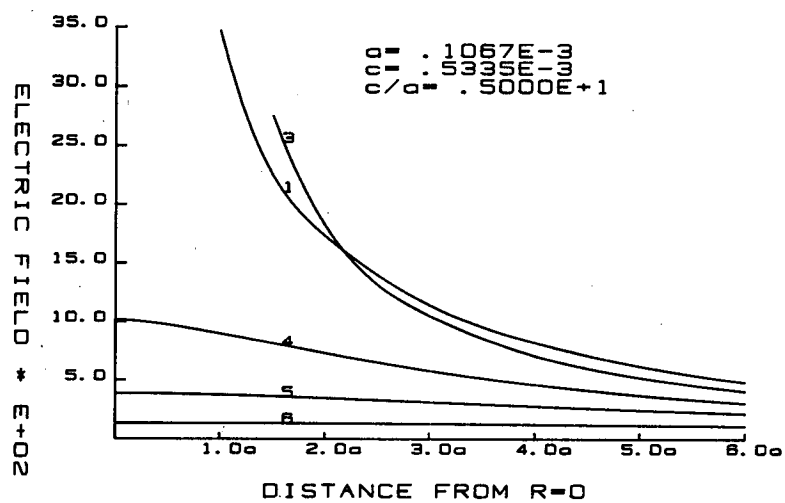

FIG. 7. As in Fig. 6 except for $b = 5.00$.

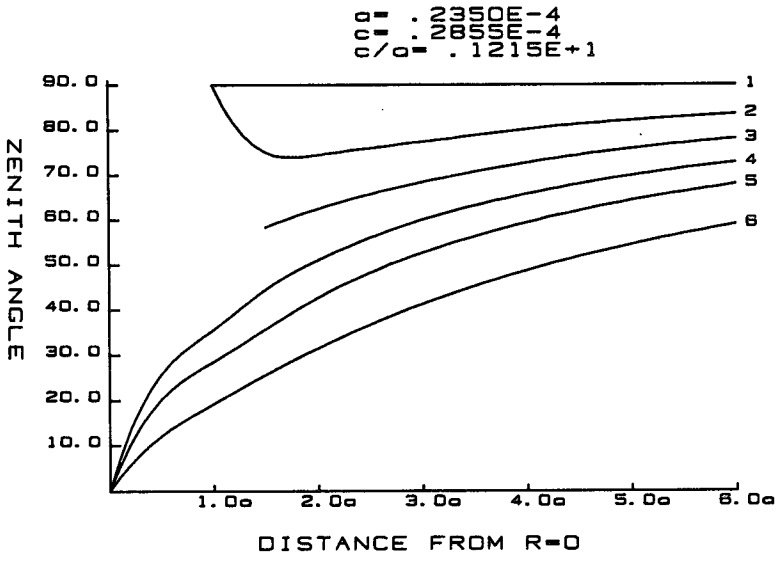

FIG. 8. Zenith angles of the electric fields for $b = 1.21$. Labels of curves are as in Fig. 4. The zenith angle is the angle between electric field vector and z-axis.

it is clear that using a prolate spheroid to approximate a columnar ice crystal would result in significant overestimate of these forces.

This, in turn, results in inaccurate estimates of the collision efficiencies of small aerosol particles or droplets with these crystals. These inaccuracies of the prolate spheroidal approximation are in addition to the fact that prolate spheroids lack two sharp edges as the real columnar crystals. In summary, it is felt that the approximation of columnar ice crystals by prolate spheroids is inadequate.

4. Temperature and vapor density fields

The temperature and vapor density fields surrounding a stationary ice crystal satisfy the same Poisson and Laplace equations as Eq. (4) with appropriate boundary conditions:

$$T = \begin{cases} T_s, & \rho_v = \rho_{v,s} \quad \text{at surface} \\ T_\infty, & \rho_v = \rho_{v,\infty} \quad \text{at infinity.} \end{cases} \tag{19}$$

The values of T_s, T_∞, $\rho_{v,s}$ and $\rho_{v,\infty}$ are all constants.

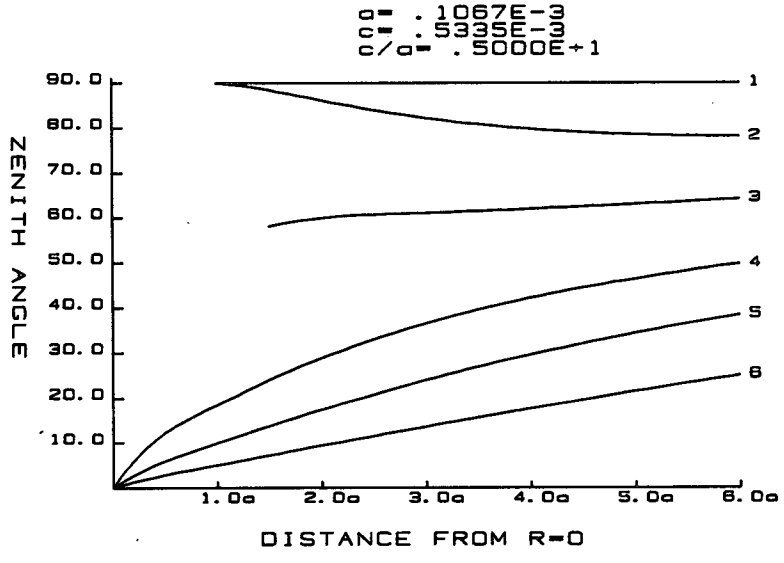

FIG. 9. As in Fig. 8 except for $b = 5.00$.

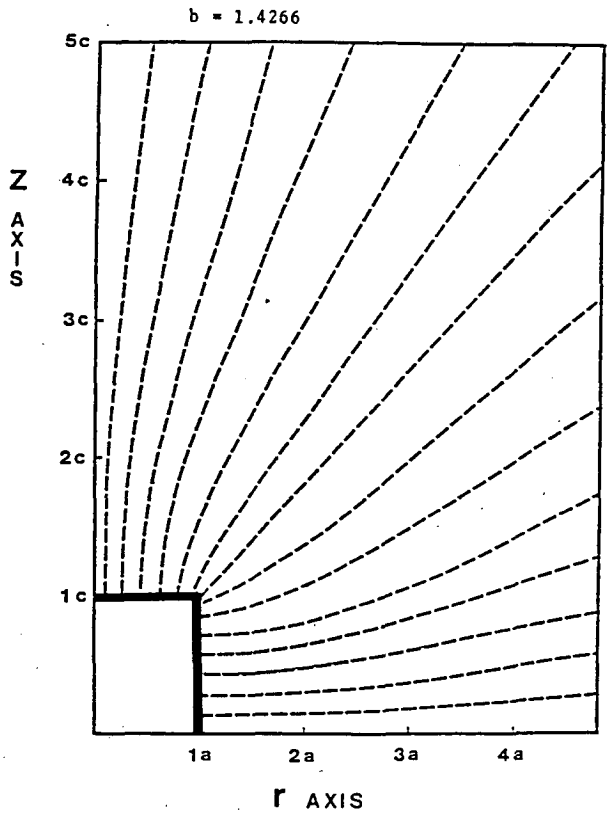

FIG. 10. Pattern of field lines for $b = 1.43$.

Although the equations are the same as the electric potential case, the boundary conditions are different. The boundary conditions for electric potential are that $V = 1$ at the surface and $V = 0$ at infinity. Therefore the preceding values of potentials and electric fields cannot be used to represent the respective temperature (vapor density) and heat flux (vapor flux) directly but must be modified by some factors. Such factors are derived in the following. Let a dimensionless quantity T' be defined as

$$T' = \frac{T - T_\infty}{T_s - T_\infty}. \tag{20}$$

Then T' also satisfies Eq. (4) with the boundary conditions for T' being

$$T' = \begin{cases} 1 & \text{at surface} \\ 0 & \text{at infinity,} \end{cases} \tag{21}$$

which are the same as that for V. Therefore the values given in Fig. 4 can be used to represent T'. The actual temperature is, of course,

$$T = (T_s - T_\infty)T' + T_\infty, \tag{22}$$

and the actual temperature gradient is

$$\nabla T = (T_s - T_\infty)\nabla T'. \tag{23}$$

Similarly,

$$\rho_v = (\rho_{v,s} - \rho_{v,\infty})\rho_v' + \rho_{v,\infty}, \tag{24}$$

$$\nabla\rho_v = (\rho_{v,s} - \rho_{v,\infty})\nabla\rho_v', \tag{25}$$

where

$$\rho_v' = \frac{\rho_v - \rho_{v,\infty}}{\rho_{v,s} - \rho_{v,\infty}}. \tag{26}$$

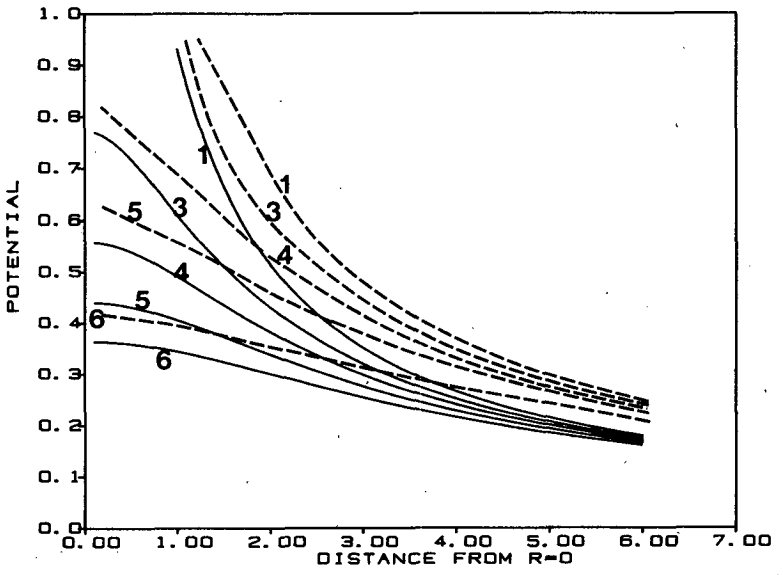

FIG. 11. Comparison of potential distributions surrounding a charged circular cylinder and a charged prolate spheroid. Dashed curves are for circular cylinder of $b = 1.21$. Solid curves are for prolate spheroid with a and c as the semi-minor and semi-major axes, respectively. Labels of curves are as in Fig. 4.

5. Conclusions

Herein we presented the methods of calculation and results of the electric, temperature, and vapor density fields surrounding columnar ice crystals. Actually any quantity satisfying the same Poisson and Laplace equations with Dirichlet boundary conditions (i.e., the values of the dependent variable at the boundaries are specified) can be treated in the same manner. The computed results should be useful in some cloud physical calculations.

It is to be noted that we treated here the cases for stationary ice crystals. The electrostatic fields will not be influenced by the motions of crystals and the values obtained above can be used directly. The temperature and vapor density fields, however, will change if ice crystals are moving. This requires the knowledge of flow fields. At present it is very difficult to calculate the flow fields caused by the motion of ice crystals which are truly three-dimensional in nature. Nevertheless, the present results can be applied to cases when flow is not important.

There are also many other shapes of snow crystals whose electric, thermal, and diffusional quantities are yet to be determined. Some of the shapes of planar hexagonal snow crystals have been mathematically modeled by Wang and Denzer (1983). Since this shape category can also be thought as "cylindrical" (except that their boundaries are not circular but are transformed by the expressions given by Wang and Denzer), it is suspected that their fields can be calculated in a similar manner once the boundary transformation is done. This is currently under our research.

Acknowledgments. The authors wish to thank anonymous reviewers for very helpful comments. We thank Eva Singer for typing this manuscript. This research is partially supported by National Science Foundation Grant ATM-8317602, University of Wisconsin-Madison Graduate Research Grant 151434 and the Environmental Protection Agency Grant R809371-01-0.

REFERENCES

Grover, S. N., H. R. Pruppacher and A. E. Hamielec, 1977: A numerical determination of the efficiency with which spherical aerosol particles collide with spherical water drops due to inertial impaction, phoretic, and electric forces. *J. Atmos. Sci.*, **34**, 1655–1669.

Morse, P. M., and H. Feshbach, 1953: *Methods of Theoretical Physics, Vol. II.*, McGraw-Hill, p. 1285.

Pruppacher, H. R., and J. D. Klett, 1978: *Microphysics of Clouds and Precipitation*, D. Reidel, 714 pp.

Schlamp, R. J., H. R. Pruppacher and A. E. Hamielec, 1975: A numerical investigation of the efficiency with which simple columnar ice crystals collide with supercooled water drops. *J. Atmos. Sci.*, **32**, 2330–2337.

Smythe, W. R., 1956: Charged right circular cylinders. *J. Appl. Phys.*, **27**, 917–920.

——, 1962: Charged right circular cylinders. *J. Appl. Phys.*, **33**, 2966–2967.

——, 1968: *Static and Dynamic Electricity*, 3rd ed., McGraw-Hill, 623 pp.

Wang, P. K., and H. R. Pruppacher, 1980: On the efficiency with which aerosol particles of radius less than 1 micron are collected by columnar ice crystals. *Pure Appl. Geophys.*, **118**, 1090–1108.

——, and C. H. Chuang, 1982: Electrical, thermal, and diffusional properties of columnar and planar ice crystals of finite length. *Preprint, Conf. Cloud Physics*, Chicago, Amer. Meteor. Soc., 338–341.

——, and S. M. Denzer, 1983: Mathematical description of the shape of plane hexagonal snow crystals. *J. Atmos. Sci.*, **40**, 1024–1028.

——, S. N. Grover and H. R. Pruppacher, 1978: On the effect of electric charges on the scavenging of aerosol particles by cloud and small rain drops. *J. Atmos. Sci.*, **35**, 1735–1743.